

# $\pi$ - and $K$ -meson properties for large $N_f$ and $N_c$

Aftab Ahmad\* and Mumtaz Khan†

*Institute of Physics, Gomal University, 29220, D.I. Khan, Khyber Pakhtunkhaw, Pakistan.*

Dynamical chiral symmetry restoration for higher number of light quark flavors  $N_f$  and breaking for higher number of colors  $N_c$  implies the suppression and enhancement of the dynamically generated quark mass. The study of various larger values of  $N_f$  and  $N_c$  may have greater impact on the internal structure of light hadrons. In this work, we study the properties of the  $\pi$ - (pion) and  $K$ -meson (kaon), such as mass, condensate, and leptonic decay constant, for various  $N_f$  and  $N_c$ . We use the symmetry-preserving vector-vector flavor-dependent contact interaction model of quark. The dynamical quark masses are calculated by using the Schwinger-Dyson equation (SDE). The masses of the pion ( $m_\pi$ ) and kaon ( $m_K$ ) for different values of  $N_f$  and  $N_c$  are determined using the homogeneous Bethe-Salpeter equation. For fixed  $N_f = 2$  and  $N_c$  is increased, the dynamically generated quark mass  $M_{u/d}$  (mass of up and down quarks), strange quark mass ( $M_s$ ), meson in-condensate  $\kappa_{(\pi,K)}^{1/3}$ , and decay constant  $f_{(\pi,K)}$  all increases. The pion mass  $m_\pi$  remains approximately constant until  $N_c$  reaches around 6.5, after which it grows rapidly. On the other hand, the kaon mass  $m_K$  increases slowly with increasing  $N_c$  until it reaches approximately  $N_c \approx 7.5$ , beyond which it rises quickly. When  $N_c = 3$  is fixed at and various values of  $N_f$  are considered, all the parameter values decrease as a function of  $N_f$ , except for the pion and kaon mass  $m_{(\pi,K)}$ , which increase above a critical value of  $N_f$  around 8. This is the region where chiral symmetry is restored, and the pion and kaon behave as free particles, similar to their behavior in the presence of a heat bath. The results obtained for fixed  $N_f = 2$  and  $N_c = 3$  are fairly in decent agreement with experimentally calculated statistics and previous model calculations based on the Schwinger-Dyson equation (SDE) and Bethe-Salpeter equation (BSE).

PACS numbers: 14.40.Aq, 24.85.1p, 11.10.St, 12.38.-t, 12.38.Lg, 12.38.Aw, 11.15.Pg

## I. INTRODUCTION

Quantum Chromodynamics (QCD) is a well-established theory that explores the fascinating world of strong color interaction between quarks and gluons. These interaction formed the bound states known as hadrons. QCD has two major regimes known as asymptotic freedom and quark confinement. Asymptotic freedom, which was discovered by Gross and Wilczek [1, 2], describes the weak interaction between quarks at high energies. On the other hand, quark confinement, as proposed by Wilson [3], explains the strong interaction between quarks at low energies, preventing them from existing in isolation. In addition to the color confinement, the dynamical chiral symmetry breaking is another significant characteristic of low-energy QCD. This concept is closely linked to the generation of constituent quark masses. It's widely recognized that QCD displays both confinement and chiral symmetry breaking when considering a small number of light quark flavors, denoted as  $N_f$ . However, for larger values of  $N_f$ , it is believed that there exists a critical value  $N_f^c$ , beyond which the chiral symmetry is restored and the quark becomes deconfined [4–6]. This critical value  $N_f^c$  must be smaller than the upper limit of the critical value, denoted as  $N_f^{A_f,c}$ , where asymptotic freedom

is believed to exist. According to the research by Politzer in 1973 [2], for a gauge group  $SU(3)$ , the critical number is  $N_f^{A_f,c} = 16.5$ . Therefore, the QCD theory is considered to be conformal in the infrared regime, driven by the presence of an infrared fixed point (the fixed point corresponds to a specific point where the  $\beta$ -functions for the QCD couplings tends to zero) [7–13]. The range of fermion flavors  $N_f^c \lesssim N_f < N_f^{A_f,c}$ , it is commonly referred to as the “conformal region” [4, 14]. As we approach the upper limit ( $N_f \lesssim N_f^{A_f,c}$ ) of this region, the infrared fixed point is situated in the weakly interacting region, However, at the lower end ( $N_f \sim N_f^c$ ), the infrared fixed point undergoes a shift towards the strongly interacting region. In this region, the coupling becomes increasingly strong as  $N_f$  decreases. Consequently, the system enters a phase characterized by the breaking of chiral symmetry and the confinement of quarks. Lattice QCD simulations [6, 15–18], as well as continuum methods of QCD [5, 19–23] and some effective models of QCD [24] in the fundamental  $SU(3)$  representation have all highlighted the significance of the chiral symmetry restoration and deconfinement phases occurring as  $N_f$  enters the conformal zone  $8 \lesssim N_f^c < 12$  and approximated the value of critical number of flavors  $N_f^c \approx 8$ . The low energy QCD theory, characterized by a larger number of colors  $N_c$  in the fundamental  $SU(N_c)$  representation, has a notable impact in the infrared regime as well. In Ref. [23, 24], it has been observed that the dynamically chiral symmetry breaks beyond a critical value of  $N_c^c \approx 2.2$  and hence the dynamically generated

\* aftabahmad@gu.edu.pk

† mkmarwat700@gmail.com

quark mass increases with the increase of  $N_c$ . In recent comprehensive analyses[24], the QCD phase diagram at finite temperature and density has been explored, with a particular focus on the influence of higher  $N_f$  and  $N_c$ . The findings indicate that the critical line separating the hadron phase from the Quark gluon plasma experiences suppression as the number of flavors increases, while it becomes more pronounced with higher values of  $N_c$ . Additionally, the rate of Schwinger quark-antiquark production exhibits a swifter growth as the number of flavors,  $N_f$ , increases, whereas it demonstrates a slower increase with rising values of  $N_c$  [25]. Exploring the impact of higher values of  $N_c$  and  $N_f$  on light hadron bound states, especially the properties of the  $\pi$ - and  $K$ -meson, would yield intriguing and meaningful results. This investigation holds great importance as it allows us to gain a deeper understanding of how these fundamental particles behave under varying conditions. Our primary objective and motivation for this endeavor and research undertaking is to explore various parameters associated with light hadrons, particularly the masses, condensate and leptonic decay constant of  $\pi$ - and  $K$ -meson, when considering a larger number of quark colors  $N_c$  and flavors  $N_f$ . The  $\pi$ - and  $K$ -meson are considered the lightest hadrons and serve as mediators for the long-range interaction between hadrons. These mesons are easily generated in collisions involving electrons and nucleons, making them ideal for investigating models of hadronic structure and sub-nucleonic degrees of freedom within nuclei. Being mesons, they consist of a simple quark-antiquark valence-quark composition, making them the simplest light-quark systems to study as bound states influenced by strong interactions. This analysis is necessary for developing a comprehensive understanding of their properties and interactions based on the elementary degrees of freedom in QCD. There is a strong motivation in electron-ion-collider (EIC) in BNL beside HERA to probe into the structure of  $\pi$ - and  $K$ -meson, see for example Ref. [26] for detail analysis. In our present investigation, we employ the Schwinger-Dyson equation to calculate the dynamical quark mass, and we utilize the homogeneous Bethe-Salpeter equation (BSE) [27] to determine the mass of the  $\pi$ - and  $K$ - meson for higher values of  $N_c$  and  $N_f$ . The homogeneous BSE can be understood as an eigenvalue problem, where the eigenvalue ( $P^2 = -m_H^2$ ) represents the square of the mass of the bound state [28]. The eigenvector in this case corresponds to the bound state amplitude. This bound state amplitude, also known as the Bethe-Salpeter amplitude, plays a vital role in the computation of production and scattering processes that involve mesons. By delving into these calculations, we aim to gain a deeper understanding of the intricacies and characteristics of light hadrons. Our gap equation and the BSE kernel will be formulated using the symmetry-preserving, confining vector-vector flavor-dependent contact interaction (FCI) model of quarks [23–25]. We will be working in the Landau gauge

and employing an optimal Schwinger-proper time regularization scheme within the rainbow-ladder truncation. This approach allows us to maintain the desired symmetries while accurately capturing the dynamics of quarks in our calculations. By utilizing these specific methods, we aim to obtain comprehensive and reliable results in our research. The article is organized as follows: In Section 2, we provide a comprehensive overview of the flavor-dependent contact interaction model and the SDE gap equation. In Sec. 3, we present the BSE approach to mesons and dynamical quark masses. Additionally, we discuss the meson bound state quark interaction model, including the flavor-dependent CI model approach and the Bethe-Salpeter amplitude (BSA) for mesons. Moving on to Section 4, we present our desired findings and results, focusing on both a higher number of flavors and colors. Lastly, in Section 5, we summarize our research and highlight the outcomes we have achieved.

## II. FLAVOR-DEPENDENT CONTACT INTERACTION MODEL AND THE GAP EQUATION

We start our discussion from the Schwinger-Dyson equations (SDE) [29], where the dressed-quark propagator  $S_f$  can be written as:

$$S_f^{-1}(p) = S_{f,0}^{-1}(p) + \Sigma(p). \quad (1)$$

Here,  $S_{f,0}(p) = (\not{p} + m_f + i\epsilon)^{-1}$ , is the bare quark propagator. The  $S_f(p) = (\not{p} + M_f + i\epsilon)^{-1}$  represents the dressed quark propagator. Where  $\Sigma(p)$  is the self-energy and is given by:

$$\Sigma(p) = \int \frac{d^4q}{(2\pi)^4} g^2 D_{\mu\nu}(q) \frac{\lambda^a}{2} \gamma_\mu S_f(q) \frac{\lambda^a}{2} \Gamma_\nu(p, q), \quad (2)$$

here  $g^2$  is the QCD coupling constant and  $\Gamma_\nu(p, q)$  is the dressed quark-gluon vertex.  $D_{\mu\nu}(q)$  is the gluon propagator and  $\lambda^a$ 's are the Gell-Mann matrices. In the  $SU(N_c)$  representation the Gell-Mann matrices satisfy the following identity :

$$\sum_{a=1}^{N_c^2-1} \frac{\lambda^a}{2} \frac{\lambda^a}{2} = \frac{1}{2} \left( N_c - \frac{1}{N_c} \right) I, \quad (3)$$

where,  $I$  is the identity matrix. In the present work, we use a symmetry-preserving confining flavor-dependent contact interaction (FCI) model [23–25] for the gluon propagator in the Landau gauge, in the infrared region where the gluons acquires a dynamically generated mass  $m_g$  [30–34]. The model is given by

$$g^2 D_{\mu\nu}(p - q) = \frac{4\pi\alpha_{\text{ir}}}{m_g^2} \sqrt{1 - \frac{(N_f - 2)}{N_f^c}} \delta_{\mu\nu} = \delta_{\mu\nu} \alpha_{\text{eff}}(N_f) \quad (4)$$

where the parameter  $\alpha_{\text{ir}} = 0.93\pi$  is the infrared-enhanced interaction strength and  $m_g = 800$  MeV is the gluon mass

scale [35]. The  $\mathcal{N}_f^c = N_f^c + \eta$  represents some guessed values of the critical number of flavors [23, 24], where the value of the parameter  $\eta$  was so adjusted to be in the range 1.8 – 2.3, to obtain the desired critical number  $N_f^c \approx 8$ , above which dynamical chiral symmetry is restored and deconfinement occurs. It has been explained and justified in Ref. [23] that the appearance of the parameter  $\eta$  is because of the factor  $(N_f - 2)$  in Eq. (4).

With a particular choice of the flavor-dependent model Eq. (4), and after performing the trace over the Dirac matrices, the dynamical quark mass function  $M_f$  is given by:

$$M_f = m_f + \frac{\alpha_{eff}^{N_c}(N_f)}{2} \int \frac{d^4 q}{(2\pi)^4} \text{Tr}[S_f(k)]. \quad (5)$$

Here  $M_f$  is the dynamical quark mass  $m_f$  is current quark mass and

$$\alpha_{eff}^{N_c}(N_f) = \frac{1}{2} \sqrt{1 - \frac{(N_f - 2)}{\mathcal{N}_f^c}} \left( N_c - \frac{1}{N_c} \right). \quad (6)$$

On simplifying Eq. (5), we get

$$M_f = m_f + 2\alpha_{eff}^{N_c}(N_f) \int \frac{d^4 q}{(2\pi)^4} \frac{M_f}{q^2 + M_f^2}. \quad (7)$$

The quark-antiquark condensate in this truncation is defined as:

$$-\langle \bar{q}q \rangle = \frac{M_f - m_f}{2\alpha_{eff}^{N_c}(N_f)}. \quad (8)$$

After setting the variable  $s = q^2$ , and using  $d^4 q = (1/2)q^2 dq^2 \sin^2 \theta d\theta \sin \phi d\phi d\psi$  in Eq. (7) and then performing the integration, we get

$$M_f = m_f + \frac{\alpha_{eff}^{N_c}(N_f)}{8\pi^2} \int_0^\infty ds \frac{s}{s + M_f^2}. \quad (9)$$

The integral mentioned in equation Eq. (9) is not convergent and requires regulation. In this study, we utilize the Schwinger proper-time regularization scheme [29] to address this issue. This procedure involves exponentiation the denominator of the integrand and introducing an additional infrared cut-off  $\tau_{ir} = 1/\Lambda_{ir}$ , alongside the conventional ultraviolet cut off  $\tau_{uv} = 1/\Lambda_{uv}$ . The integrand of Eq. (9) can be written as

$$\begin{aligned} \frac{1}{s + M_f^2} &= \int_0^\infty d\tau e^{-\tau(s + M_f^2)} \rightarrow \int_{\tau_{uv}^2}^{\tau_{ir}^2} d\tau e^{-\tau(s + M_f^2)} \\ &= \frac{e^{-\tau_{uv}^2(s + M_f^2)} - e^{-\tau_{ir}^2(s + M_f^2)}}{s + M_f^2}. \end{aligned} \quad (10)$$

The infrared cutoff  $\tau_{ir}$  is employed to implement confinement by ensuring the absence of quark production thresholds [36–39]. However, it is important to note that the CI

model, as described in Eq. (9), is a non-renormalizable theory. This means that the parameter  $\tau_{uv}$ , cannot be eliminated and instead becomes an integral part of the model. It sets the scale for all dimensional quantities within the model. Furthermore, the ultraviolet cutoff  $\Lambda_{uv}$ , also plays a significant role in the study of heavier quarks. By increasing  $\Lambda_{uv}$ , we can simulate the short-distance effects that occur as the quark mass increases. The adoption of this regularization procedure is significant as it eliminates quadratic and logarithmic divergences and ensures satisfaction of the axial-vector Ward-Takahashi identity [40, 41]. From Eq. (9) and Eq. (10) and after performing the integration over ‘s’, the gap equation is reduced to:

$$M_f = m_f + \frac{M_f \alpha_{eff}^{N_c}(N_f)}{8\pi^2} \mathcal{A}_{01}(M_f^2, \tau_{uv}^2, \tau_{ir}^2), \quad (11)$$

with

$$\mathcal{A}_{\delta\zeta}(M^2; \tau_{uv}^2, \tau_{ir}^2) = \frac{(M_f^2)^\epsilon}{\Gamma(\zeta)} \Gamma(\zeta - 2, \tau_{uv}^2 M^2, \tau_{ir}^2 M^2), \quad (12)$$

where  $\epsilon = \delta - (\zeta - 2)$  and  $\Gamma(a, y_1, y_2) = \Gamma(a, y_1) - \Gamma(a, y_2)$  with  $\Gamma(a, y) = \int_y^\infty t^{a-1} e^{-t} dt$  being the incomplete Gamma function. In this FCI model, the confinement for higher  $N_c$  and  $N_f$  can be triggered from the confining length scale [23, 25, 42–44]:

$$\tilde{\tau}_{ir} = \tau_{ir} \frac{M(3, 2)}{M(N_c, N_f)}, \quad (13)$$

here  $M(3, 2)$  is the dynamical mass for fixed  $N_c = 3$  and  $N_f = 2$ .  $M(N_c, N_f)$  is the generalized  $N_c$  and  $N_f$  dependent dynamical mass. The model introduces the parameter  $\tau_{ir}$  to simulate confinement by ensuring the absence of quark production thresholds. In the presence of  $N_f$  and  $N_c$ ,  $\tau_{ir}$  needs to vary slightly with both  $N_f$  and  $N_c$ . Therefore, the connection between dynamical chiral symmetry breaking and confinement is expressed through a regulator, denoted as  $\tilde{\tau}_{ir}$ , which explicitly depends on  $N_f$  and  $N_c$ . The confinement length scale, as described in Eq. (13), becomes infinite when chiral symmetry is restored in the chiral limit. This leads to deconfinement at a certain critical value  $N_f^c$ , where the production thresholds reappear [23, 25]. In the next section we discuss the general formalism for BSE with FCI Model.

### III. BETHE-SALPETER EQUATION FOR PSEUDOSCALAR MESON AND THE FCI MODEL

A comprehensive relativistic approach to meson bound states is facilitated by the Bethe-Salpeter equation (BSE). The BSE reveals poles in the four-point function, which correspond to the existence of meson-bound states. The homogeneous BSE establishes the conditions necessary for these poles to emerge in a specific  $J^{PC}$  channel.

Since quarks cannot be directly observed in high-energy experiments, the study of bound states becomes crucial for testing QCD. Specifically, the determination of a meson bound-state problem in a specific  $J^{PC}$  channel relies on its homogeneous counterpart and is given by:

$$[\Gamma_H(k; P)]_{tu} = \int \frac{d^4q}{(2\pi)^4} K_{tu;rs}(k, q; P) \chi(q; P)_{sr}, \quad (14)$$

with

$$\chi(q; P) = S_f(q_+) \Gamma_H(q; P) S_g(q_-), \quad (15)$$

is the Bethe-Salpeter wave-function and  $q_+ = q + \eta P$ ,  $q_- = q - (1 - \eta)P$ ;  $\eta \in [0, 1]$  is a momentum-sharing parameter. Here  $k$  is the relative and  $P$  is the total momentum of the quark-antiquark system.  $\Gamma_H(k; P)$  represents the meson Bethe-Salpeter amplitude (BSA). The symbol  $H = f\bar{g}$  denotes the quantum numbers and flavor composition of the meson, and  $r, s, t$ , and  $u$  represent color, flavor, and spinor indices respectively. As previously stated,  $S_f$  is the dressed-quark propagator and  $K(k, q; P)$  is the quark-antiquark scattering kernel. The study of the pseudoscalar meson (i.e., pions, kaons etc.) observables lacks significance unless it explicitly ensures the satisfaction of the vector and axial-vector Ward-Takahashi identities (axWTI) [45]. In the chiral limit ( $m_f = 0$ ), the axWTI can be written as:

$$-P_\mu \Gamma_{5\mu}(k; P) = S^{-1}(k_+) \gamma_5 + \gamma_5 S^{-1}(k_-). \quad (16)$$

Where  $k_+ = k + P$ ,  $k_- = k$  and  $\Gamma_{5\mu}(k, P)$  is the axial vector vertex, which is determined by

$$\Gamma_{5\mu}(k; P) = \gamma_5 \gamma_\mu + \int \frac{d^4q}{(2\pi)^4} K(k, q; P) \chi_{5\mu}(q_+, q). \quad (17)$$

Eq. (16), which capture the phenomenological aspects of dynamical chiral symmetry breaking (DCSM) in QCD, it is essential to establish a connection between the axial-vector vertex, denoted as  $\Gamma_{5\mu}(k; P)$ , and the quark propagator, represented as  $S_f(k)$ . This connection implies a correlation between the kernel in the BSE Eq. (16) and the kernel in the quark SDE Eq. (1). Any truncation scheme applied to the SDE-BSE coupled system must preserve this relationship, thereby influencing the characteristics of the quark-antiquark scattering kernel  $K(p, q; P)$ . In the context of the contact interaction (CI) and rainbow-ladder truncation (bare-vertex approximation) [38, 45, 46], the  $K(p, q; P)$  is given as:

$$K(p, q; P) = -g^2 D_{\mu\nu}(p - q) \left[ \frac{\lambda^a}{2} \gamma_\mu \right] \otimes \left[ \frac{\lambda^a}{2} \gamma_\nu \right], \quad (18)$$

Upon inserting Eq. (3) and Eq. (4) in Eq. (18) and then using in Eq. (14), we have the homogeneous BSE ( $\eta = 1$ ), in the FCI model Eq. (6), for ground state pseudoscalar meson ( $J^{PC} = 0^{-+}$ ) can be expressed as:

$$\Gamma_{0^{-+}}(k; P) = -4\alpha_{\text{eff}}^{N_c}(N_f) \int \frac{d^4q}{(2\pi)^4} \quad (19)$$

$$\gamma_\mu S_f(q + P) \Gamma_{0^{-+}}(q; P) S_{\bar{g}}(q) \gamma_\mu. \quad (20)$$

In the FCI symmetry preserving regularization scheme and in the rainbow-ladder truncation the Bethe-Salpeter amplitude cannot depend on relative momentum ( see for example for the detail analysis [38, 46]). A general decomposition for pseudoscalar meson in the FCI scenario has the following form:

$$\Gamma_{0^{-+}}(P) = i\gamma_5 E_{0^{-+}}(P) + \frac{1}{M_R} \gamma_5 \gamma \cdot P F_{0^{-+}}(P), \quad (21)$$

where  $M_R = M_f M_{\bar{g}} / (M_f + M_{\bar{g}})$ ,  $E_{0^{-+}}(P)$  and  $F_{0^{-+}}(P)$  are the Bethe-Salpeter amplitudes (BSA). Substituting Eq. (21) in Eq. (20), and by adopting the same procedure described in Refs. [38, 46–49] allows for the easy derivation of the explicit expression for the BSE of the pseudoscalar mesons. To ensure the preservation of Eq. (16), it is necessary to incorporate a regularization technique. This necessity leads us to the following form of the axWTI [38, 46–49]:

$$0 = \int_0^1 d\alpha \int \frac{d^4q}{(2\pi)^4} \frac{\frac{1}{2}q^2 + \mathcal{W}}{[q^2 + \mathcal{W}]^2}, \quad (22)$$

where  $\alpha$  is a Feynman parameter and  $\mathcal{W} = \mathcal{W}(M_g, M_f, \alpha, P^2) = M_g^2(1 - \alpha) + M_f^2\alpha + \alpha(1 - \alpha)P^2$ . Eq. (22) can be further simplified as

$$0 = \int_0^1 d\alpha \{ \mathcal{A}_{01}(\mathcal{W}) + \mathcal{A}_{02}(\mathcal{W}) \}, \quad (23)$$

with  $\mathcal{A}_{02}(x) = -x(d/dx)\mathcal{A}_{01}(x)$  and  $\bar{\mathcal{A}}_{02}(x) = \mathcal{A}_{02}(x)/x$ . Now we can write the explicit form of the Bethe-Salpeter equation Eq. (20) in the FCI model as:

$$\begin{pmatrix} E_{0^{-+}}(P) \\ F_{0^{-+}}(P) \end{pmatrix} = \frac{\alpha_{\text{eff}}^{N_c}(N_f)}{\pi^2} \begin{pmatrix} \mathcal{K}_{EE}^{0^{-+}} & \mathcal{K}_{EF}^{0^{-+}} \\ \mathcal{K}_{FE}^{0^{-+}} & \mathcal{K}_{FF}^{0^{-+}} \end{pmatrix} \begin{pmatrix} E_{0^{-+}}(P) \\ F_{0^{-+}}(P) \end{pmatrix}, \quad (24)$$

Eq. (24) is an Eigenvalue equation which has a solution at  $P^2 = -m_{0^{-+}}^2$ , with  $m_{0^{-+}}$  is the mass of pseudoscalar meson. The explicit form of the Kernels of the BSE Eq. (24) for the pseudoscalar meson (See for example for detail Appendix A of Ref. [47] and Ref. [49]) are:

$$\mathcal{K}_{EE}^{0^{-+}} = \int_0^1 d\alpha \{ \mathcal{A}_{01}(\mathcal{W}) - [M_{\bar{g}} M_f + \alpha(1 - \alpha)P^2 - \mathcal{W}] \bar{\mathcal{A}}_{02}(\mathcal{W}) \},$$

$$\mathcal{K}_{EF}^{0^{-+}} = \frac{P^2}{2M_R} \int_0^1 d\alpha [M_{\bar{g}}(1 - \alpha) + M_f \alpha] \bar{\mathcal{A}}_{02}(\mathcal{W}),$$

$$\mathcal{K}_{FF}^{0^{-+}} = -\frac{1}{2}m^2 \int_0^1 d\alpha [M_f M_{\bar{g}} + M_{\bar{g}}^2(1 - \alpha) + M_f^2 \alpha] \bar{\mathcal{A}}_{02}(\mathcal{W}),$$

$$\mathcal{K}_{FE}^{0^{-+}} = -\frac{2M_R}{P^2} \mathcal{K}_{EF}^{0^{-+}}. \quad (25)$$

For the purpose of computation of the observable, the BSA has to be normalized. In the rainbow ladder truncation of the BSE, the normalization condition (we assume  $\eta = 1$ ) is of the form:

$$P_\mu = \alpha^{N_c} \int \frac{d^4 q}{(2\pi)^4} \text{Tr}[\Gamma_{0^{--}}(-Q) \times \frac{\partial}{\partial P_\mu} S_f(q+P) \Gamma_{0^{--}}(Q) S_{\bar{g}}(q)], \quad (26)$$

where  $\alpha^{N_c}$  is the color factor in the  $SU(N_c)$  representation as discussed in Eq. (3). The condition Eq. (26) can be further simplified as:

$$1 = \frac{d}{dP^2} 2\alpha^{N_c} \int \frac{d^4 q}{(2\pi)^4} \times \text{Tr}[\Gamma_{0^{--}}(-Q) S_f(q+P) \Gamma_{0^{--}}(Q) S_{\bar{g}}(q)], \quad (27)$$

with  $P^2 = -m_{0^{--}}^2$ , where  $m_{0^{--}}$  represents the mass of pseudoscalar meson and at  $P = Q$ . By utilizing the amplitudes and propagators, it is possible to calculate various characteristics of the pseudoscalar mesons (the  $\pi$ -meson and  $K$ -meson in the present case) within the rainbow ladder truncation. This includes the leptonic decay constants and the condensates for the mesons. The decay constant in terms of canonically normalized amplitudes can be expressed as:

$$f_{0^{--}} P_\mu = \alpha^{N_c} \int \frac{d^4 q}{(2\pi)^4} \text{Tr}[\gamma_5 \gamma_\mu S(q_+) \Gamma_{0^{--}}(P) S(q_-)], \quad (28)$$

or on simplifying we have (see for example [50]):

$$f_{0^{--}} = \frac{1}{M_R} \frac{\alpha^{N_c}}{4\pi^2} [E_{0^{--}} \mathcal{K}_{FE}^{0^{--}} + F_{0^{--}} \mathcal{K}_{FF}^{0^{--}}], \quad (29)$$

and the in-meson condensate (see for an instance for detail discussion in Refs. [28, 46, 51]) is given by:

$$\kappa_{0^{--}} = f_{0^{--}} \frac{1}{M_R} \frac{\alpha^{N_c}}{4\pi^2} [E_{0^{--}} \mathcal{K}_{EE}^{0^{--}} + F_{0^{--}} \mathcal{K}_{EF}^{0^{--}}]. \quad (30)$$

In the next section, we discuss the numerical solution of the SDE-BSE to calculate the properties of  $\pi$ -meson and  $K$ -meson for higher number of light quark flavors  $N_f$  and higher number of color  $N_c$  in the fundamental  $SU(N_c)$  representation from FCI model.

#### IV. NUMERICAL RESULTS

In this section, we present our numerical results and discussion. We will be utilizing the technique of flavor dependent contact interaction with renormalized SDE for the dynamical masses of up ( $u$ ), down ( $d$ ) and strange ( $s$ ) quarks and homogeneous BSE for the masses of  $\pi$  and  $K$ -meson. It is important to note that in this work, we will be discussing different possibilities for the masses

TABLE I. Parameters of the FCI model used as inputs for the SDE and BSE. These parameters were determined to reproduced the properties of ground state  $\pi$ - and  $\rho$ -mesons (for  $N_f = 2$  and  $N_c = 3$ ) in Ref. [46] and for  $K$ -meson in [50], except an additional parameter in FCI model which was determined in [23]. All the enlisted dimensioned quantities are in GeV.

$m_{u=d}$	$m_s$	$\Lambda_{ir}$	$\Lambda_{uv}$	$\alpha_{ir}$	$m_g$	$N_f^c$
0.007	0.17	0.24	0.905	$0.93\pi$	0.8	9.98

TABLE II. In the following table we presents the solution of the SDE and the BSE and calculated all these physical quantities for fixed  $N_f = 2$  and  $N_c = 3$ . All the computed quantities are in the units GeV.

$M_{u/d}$	$M_s$	$m_\pi$	$m_k$	$f_\pi$	$f_k$	$\kappa_\pi^{1/3}$	$\kappa_K^{1/3}$
0.367	0.533	0.139	0.499	0.101	0.111	0.243	0.247

of light hadrons. Firstly, we will vary the number of flavors  $N_f$ , while keeping  $N_c = 3$  fixed. Then, we will keep the value of  $N_f = 2$  fixed and vary  $N_c$ . We will consider both scenarios and compute the dynamical quark masses of  $u$ -,  $d$ -, and  $s$ -quarks, the mass of  $\pi$ -meson, the mass of  $K$ -meson, the pion decay constant  $f_\pi$ , the kaon decay constant  $f_K$ , the pion condensate  $\kappa_\pi^{1/3}$  and the kaon condensate  $\kappa_K^{1/3}$ . All the model parameters to be used in the model are enlisted in Table I. To check the consistency of our results we first fixed  $N_f = 2$  and  $N_c = 3$  and obtained the mentioned properties of the  $\pi$ - and  $K$ -meson with the FCI Model from SDE-BSE equations and enlisted the results in Table II. Our results in this scenario from FCI model are consistent with results obtained from CI model [46, 50, 52–54]. In the next subsection, we fixed  $N_f = 2$  and increase the number of color  $N_c$  and will discuss the results.

#### A. Properties of $\pi$ - and $K$ -meson for a various $N_c$

In this subsection, we present the numerical results of the SDE and BSE for a higher number of  $N_c$  while keeping  $N_f = 2$  fixed. The dynamical quark mass  $M_{u/d}$  with a bare quark mass of  $m = 0.007$  GeV is plotted in Fig. 1(a), and the dynamical strange quark mass  $M_s$  with a bare strange quark mass of  $m_s = 0.17$  GeV is shown in Fig. 1(b). These plots indicate that the dynamical mass grows rapidly above a critical value of  $N_c^c \approx 2.2$ , beyond which the dynamical chiral symmetry is broken. The critical value can be calculated from the color-gradient of the mass function  $\partial_{N_c} M$  [24, 44]. The in-meson condensate Eq. (30), for pion represented by  $\kappa_\pi^{1/3}$ , is shown in Fig. 2(a) as a function of  $N_c$ . Similarly, the condensate for kaon  $\kappa_K^{1/3}$  is presented in Fig. 2(b), both plots demonstrate the evolution of the condensates as  $N_c$  increases. The decay constant given in Eq. (29) for the

pion  $f_\pi$ , is plotted in the Fig. 3(a) as a function of  $N_c$ , while Fig. 3(b) displays the kaon decay constant  $f_K$  for various  $N_c$ . Both plots exhibit a smooth growth as  $N_c$  increases. Lastly, the mass of the pion  $m_\pi$  is plotted as a function of  $N_c$  in Fig. 4(a), where it remains nearly constant until  $N_c \approx 6.5$  and then rapidly increases. The mass of the kaon  $m_K$  is plotted in Fig. 4(b), also slightly increases as  $N_c$  increases until it reaches  $N_c \approx 7.5$  where it rises up rapidly. One of the differences in the behavior of the pion mass  $m_\pi$  and the kaon mass  $m_K$  is that the strange quark mass has a higher bare quark mass compared to the light up (or down) bare quark mass. We have compiled a Table IV with all the parameter values for different values of  $N_c$  and a fixed  $N_f = 2$ . In the following subsection, we will keep  $N_c = 3$  fixed and vary  $N_f$ .

### B. Properties of $\pi$ - and $K$ - meson for various $N_f$

In this subsection, we present the numerical solution of the SDE and the BSE for a higher number of flavors, denoted as  $N_f$ , while keeping the number of colors  $N_c = 3$  fixed. The dynamical quark mass,  $M_{u/d}$ , with a bare quark mass of  $m = 0.007$  GeV, is plotted as a function of  $N_f$  in Fig. 5(a). This plot illustrates that the dynamical mass for the light quarks,  $M_{u/d}$ , decreases monotonically as  $N_f$  increases, until it reaches a critical value of approximately  $N_f^c \approx 8$ . Beyond this critical value, the dynamical chiral symmetry is restored, and the bare quark mass remains. The critical value can be determined from the flavor-gradient of the mass function,  $\partial_{N_f} M_{u/d}$  [24, 25]. The dynamical strange quark mass  $M_s$  with bare strange quark mass  $m_s = 0.17$  GeV is shown in the Fig. 5(b), this plot shows that the  $M_s$  monotonically decreases as we increase  $N_f$  till the critical  $N_f^c \approx 11.97$ , where the dynamical mass vanishes and the bare strange quark mass survives. The critical number in the case of  $s$ -quarks is higher than that of the  $u$ - or  $d$ -quark is because of its heavier bare mass. The pion condensate  $\kappa_\pi^{1/3}$  as a function of  $N_f$  is depicted in the Fig. 6(a) whereas  $\kappa_K^{1/3}$  is presented in the Fig. 6(b), both plots shows the monotonically decrease of both the condensate as we increase  $N_f$ . The decay constant  $f_\pi$  as a function of the number of  $N_f$  is depicted in Fig. 7(a) and in the Fig. 7(b) we show the plot of  $f_K$  as a function of higher  $N_f$ . Both plots shows the monotonic decrease with an increase of  $N_f$ . We plotted the mass of pion  $m_\pi$  as function of  $N_f$  in Fig. 8(a), it remains almost constant until  $N_f \approx 8$  and above it rises rapidly in the chiral symmetry restoration region. In Fig. 8(b), we show the evolution of mass of kaon  $m_K$ , it slightly increase as we increase  $N_f$  until it grows up to higher values. The situation is quite similar to that of finite temperature where the masses of pion or kaon smoothly rises up at the chiral symmetry restoration temperature [55, 56]. We have tabulated all the parameters values for various  $N_f$  and for fixed  $N_c = 3$  in Table IV.

## V. SUMMARY AND PERSPECTIVES

In this research paper, we have conducted a study on the properties of the  $\pi$ - and  $K$ -meson, including their mass, condensate, and leptonic decay constant, considering various values of  $N_f$  and  $N_c$ . To accomplish this, we have utilized the symmetry-preserving vector-vector flavor-dependent contact interaction (FCI) model of quarks. By employing the Schwinger-Dyson equation (SDE), we have determined the dynamical quark masses  $M_{u/d}$  for the up or down quark (with  $m_u = m_d = 0.007$  GeV to maintain isospin symmetry) and the dynamical mass of the strange quark  $M_s$  (with  $m_s = 0.17$  GeV), considering different values of  $N_f$  and  $N_c$ . Additionally, we have computed the masses of the pion  $m_\pi$  and kaon  $m_K$  for various values of  $N_f$  and  $N_c$  using the homogeneous Bethe-Salpeter equation. Initially, we conducted calculations on the properties of the  $\pi$  and  $K$ -meson with fixed values of  $N_f = 2$  and  $N_c = 3$ . Our findings align with previous model calculations based on the Schwinger-Dyson equation (SDE) and Bethe-Salpeter equation (BSE). Subsequently, we kept  $N_f = 2$  constant and varied  $N_c$ , leading us to observe that the dynamically generated quark mass  $M_{u/d}$ ,  $M_s$ , the condensate  $\kappa_{(\pi,K)}^{1/3}$ , the decay constant  $f_{(\pi,K)}$ , all increase as  $N_c$  is raised. This can be attributed to the fact that a larger  $N_c$  tends to enhance the dynamical chiral symmetry. Conversely, the pion mass  $m_\pi$  remains relatively stable until  $N_c$  reaches approximately 6.5, after which it experiences a rapid increase. On the other hand, the kaon mass  $m_K$  exhibits a slight rise with increasing  $N_c$  until it reaches around  $N_c \approx 7.5$ , beyond which it increases rapidly. Next, we kept  $N_c = 3$  fixed and varied  $N_f$ . We observed that all parameter values decrease as a function of  $N_f$ , except for the pion and kaon masses  $m_{(\pi,K)}$ , which rise near the chiral symmetry restoration region (near and above a critical value of  $N_f \approx 8$ ). This region is where chiral symmetry is restored, and the pion and kaon behave as free particles, similar to their behavior in the presence of a heat bath. Therefore, according to the FCI Model prediction, the masses of the  $\pi$ - and  $K$  meson increase with larger  $N_c$  and  $N_f$ . However, the dynamical quark masses of  $u$ ,  $d$ , and  $s$  quarks, decay constant  $f_{\pi,K}$ , and meson in-condensate  $\kappa_{(\pi,K)}^{1/3}$  increase as we increase  $N_c$ , while they decrease when we increase  $N_f$ . In the near future, we are interested in extending this work to calculate the electromagnetic form factors for higher  $N_c$  and  $N_f$ .

## ACKNOWLEDGMENTS

We acknowledge A. Bashir, B.Masud and M.A. Bedolla for their guidance and suggestion. We also grateful to the colleagues of the Institute of Physics, Gomal University for their hospitality and support.

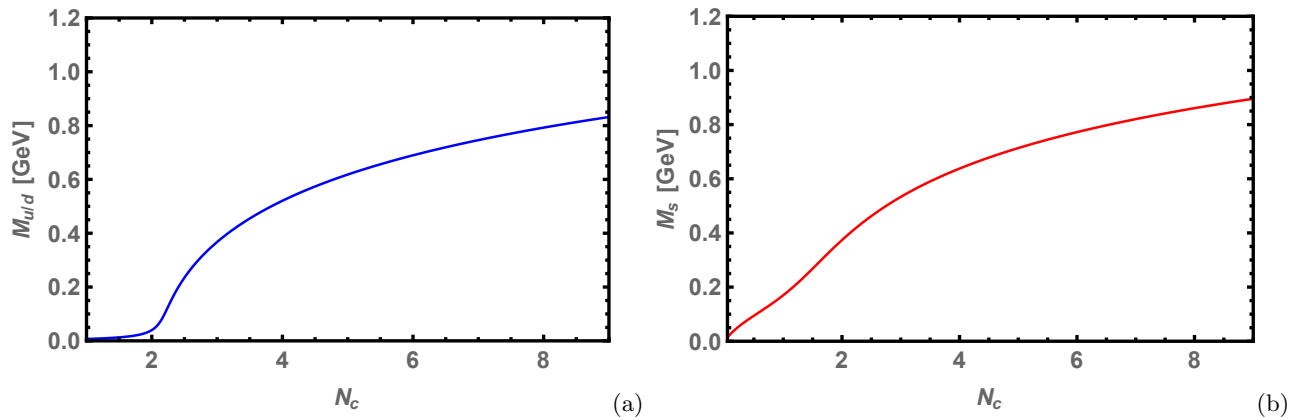


FIG. 1. (a) Behavior of the dynamical quark mass  $M_{u/d}$  as a function of the number of colors  $N_c$ , for fixed number of flavors  $N_f = 2$ , and with bare quark mass  $m_{u/d} = 0.007$  GeV. The dynamical quark mass increases as  $N_c$  increases at and above some critical value  $N_c^f \geq 2.2$ , the dynamical chiral symmetry is broken. (b) Behavior of the dynamical strange quark mass  $M_s$  with  $m_s = 0.17$  GeV as a function of  $N_c$ .

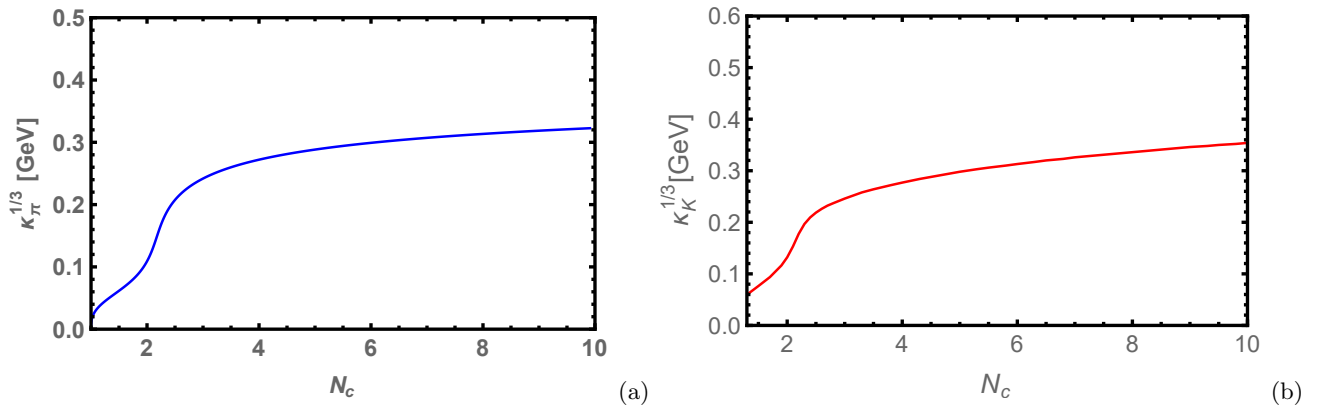


FIG. 2. (a) Behavior of pion condensate as a function of the number of colors  $N_c$  for fixed  $N_f = 2$ . (b) Behavior of the kaon condensate as a function of  $N_c$ , while keeping  $N_f = 2$  fixed.

- 
- [1] D. J. Gross and F. Wilczek, Phys. Rev. Lett. **30**, 1343 (1973).  
[2] H. D. Politzer, Phys. Rev. Lett. **30**, 1346 (1973).  
[3] K. G. Wilson, Phys. Rev. D **10**, 2445 (1974).  
[4] T. Appelquist, G. T. Fleming, and E. T. Neil, Phys. Rev. D **79**, 076010 (2009), arXiv:0901.3766 [hep-ph].  
[5] A. Bashir, A. Raya, and J. Rodriguez-Quintero, Physical Review D **88**, 054003 (2013).  
[6] T. Appelquist *et al.* (LSD), Phys. Rev. D **90**, 114502 (2014), arXiv:1405.4752 [hep-lat].  
[7] W. E. Caswell, Phys. Rev. Lett. **33**, 244 (1974).  
[8] T. Banks and A. Zaks, Nucl. Phys. B **196**, 189 (1982).  
[9] H. Gies and J. Jaeckel, The European Physical Journal C-Particles and Fields **46**, 433 (2006).  
[10] T. Appelquist, G. T. Fleming, and E. T. Neil, Phys. Rev. Lett. **100**, 171607 (2008), [Erratum: Phys.Rev.Lett. 102, 149902 (2009)], arXiv:0712.0609 [hep-ph].  
[11] A. Hasenfratz, Physical Review D **82**, 014506 (2010).  
[12] Y. Aoki, T. Aoyama, M. Kurachi, T. Maskawa, K.-i. Nagai, H. Ohki, A. Shibata, K. Yamawaki, and T. Yamazaki, arXiv preprint arXiv:1202.4712 (2012).  
[13] N. Evans and K. S. Rigatos, Phys. Rev. D **103**, 094022 (2021), arXiv:2012.00032 [hep-ph].  
[14] T. Appelquist *et al.* (LSD), Phys. Rev. Lett. **104**, 071601 (2010), arXiv:0910.2224 [hep-ph].  
[15] M. Hayakawa, K. I. Ishikawa, Y. Osaki, S. Takeda, S. Uno, and N. Yamada, Phys. Rev. D **83**, 074509 (2011), arXiv:1011.2577 [hep-lat].  
[16] A. Cheng, A. Hasenfratz, G. Petropoulos, and D. Schaich, JHEP **07**, 061 (2013), arXiv:1301.1355 [hep-lat].  
[17] A. Hasenfratz and D. Schaich, JHEP **02**, 132 (2018), arXiv:1610.10004 [hep-lat].  
[18] T. Appelquist *et al.* (Lattice Strong Dynamics), Phys. Rev. D **99**, 014509 (2019), arXiv:1807.08411 [hep-lat].  
[19] T. Appelquist, A. G. Cohen, and M. Schmaltz, Phys. Rev. D **60**, 045003 (1999), arXiv:hep-th/9901109.  
[20] M. Hopfer, C. S. Fischer, and R. Alkofer, JHEP **11**, 035 (2014), arXiv:1405.7031 [hep-ph].

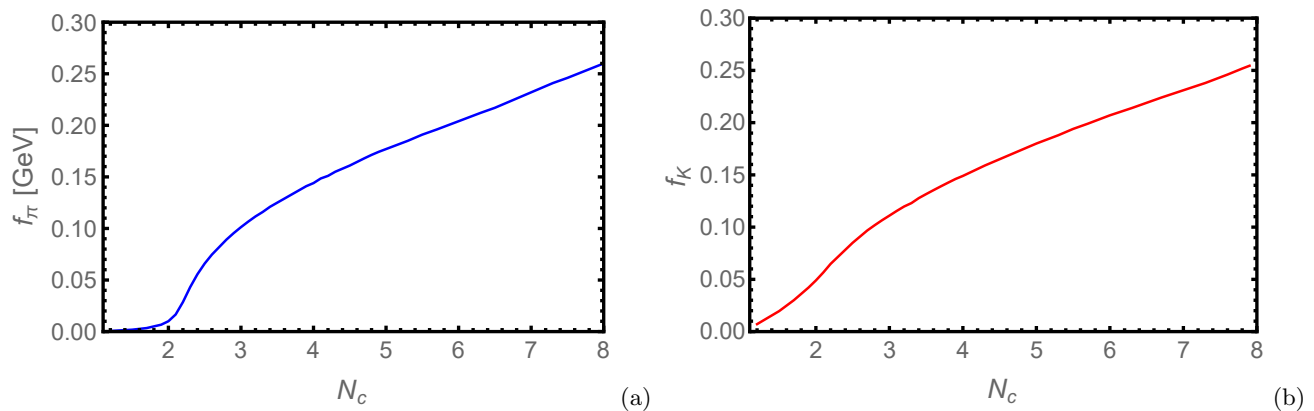


FIG. 3. (a) The variation of the pion decay constant for various  $N_c$  at fixed  $N_f = 2$ . (b) The variation of the kaon decay constant for various  $N_c$  at fixed  $N_f = 2$ .

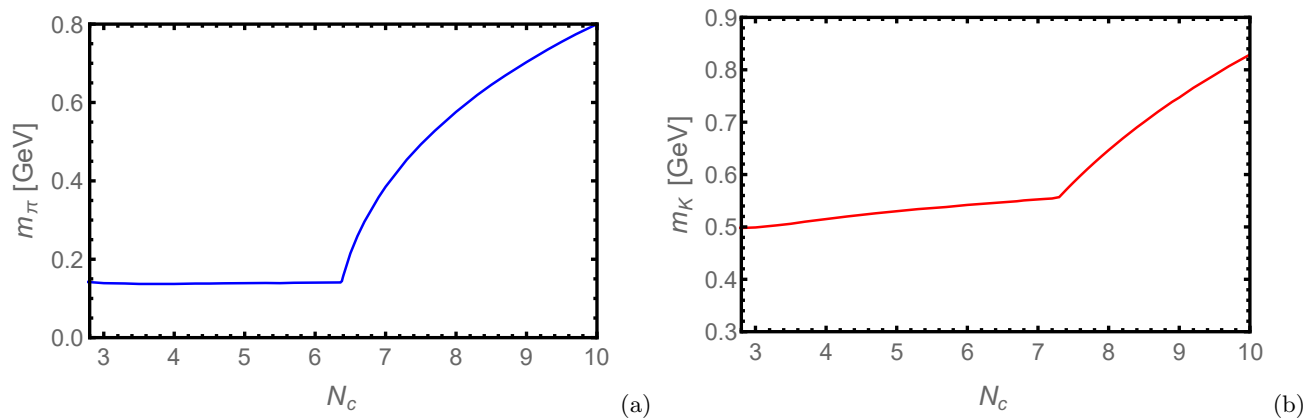


FIG. 4. (a) The Behavior of pion mass  $m_\pi$  with  $N_c$ , while keeping  $N_f = 2$ . The pion mass approximately constant until  $N_c \approx 6.5$  while above it rises quickly. (b) Behavior of the kaon mass  $m_\kappa$  as a function of  $N_c$ , while keeping  $N_f = 2$  fixed. It slowly rises till  $N_c \approx 7.5$  where above it grows faster.

- [21] A. Doff and A. A. Natale, Phys. Rev. D **94**, 076005 (2016), arXiv:1610.02564 [hep-ph].
- [22] D. Binosi, C. D. Roberts, and J. Rodriguez-Quintero, Phys. Rev. D **95**, 114009 (2017), arXiv:1611.03523 [nucl-th].
- [23] A. Ahmad, A. Bashir, M. A. Bedolla, and J. J. Cobos-Martínez, J. Phys. G **48**, 075002 (2021), arXiv:2008.03847 [hep-ph].
- [24] A. Ahmad and A. Murad, Chin. Phys. C **46**, 083109 (2022), arXiv:2201.09980 [hep-ph].
- [25] A. Ahmad and A. Farooq, (2023), arXiv:2302.13265 [hep-ph].
- [26] A. C. Aguilar *et al.*, Eur. Phys. J. A **55**, 190 (2019), arXiv:1907.08218 [nucl-ex].
- [27] E. E. Salpeter and H. A. Bethe, Phys. Rev. **84**, 1232 (1951).
- [28] P. Maris and C. D. Roberts, Phys. Rev. C **56**, 3369 (1997), arXiv:nucl-th/9708029.
- [29] J. S. Schwinger, Phys. Rev. **82**, 664 (1951).
- [30] K. Langfeld, C. Kettner, and H. Reinhardt, Nucl. Phys. A **608**, 331 (1996), arXiv:hep-ph/9603264.
- [31] J. M. Cornwall, Phys. Rev. D **26**, 1453 (1982).
- [32] A. C. Aguilar, D. Binosi, and J. Papavassiliou, Front. Phys. (Beijing) **11**, 111203 (2016), arXiv:1511.08361 [hep-ph].
- [33] L. X. Gutierrez-Guerrero, A. Bashir, I. C. Cloet, and C. D. Roberts, Phys. Rev. **C81**, 065202 (2010), arXiv:1002.1968 [nucl-th].
- [34] H. Kohyama, (2016), arXiv:1602.09056 [hep-ph].
- [35] P. Boucaud, J. P. Leroy, A. L. Yaouanc, J. Micheli, O. Pene, and J. Rodriguez-Quintero, Few Body Syst. **53**, 387 (2012), arXiv:1109.1936 [hep-ph].
- [36] D. Ebert, T. Feldmann, and H. Reinhardt, Phys. Lett. **B388**, 154 (1996), arXiv:hep-ph/9608223 [hep-ph].
- [37] C. D. Roberts, M. S. Bhagwat, A. Holl, and S. V. Wright, Eur. Phys. J. ST **140**, 53 (2007), arXiv:0802.0217 [nucl-th].
- [38] H. L. L. Roberts, L. Chang, I. C. Cloet, and C. D. Roberts, Few Body Syst. **51**, 1 (2011), arXiv:1101.4244 [nucl-th].
- [39] H. L. L. Roberts, A. Bashir, L. X. Gutierrez-Guerrero, C. D. Roberts, and D. J. Wilson, Phys. Rev. **C83**, 065206 (2011), arXiv:1102.4376 [nucl-th].
- [40] J. C. Ward, Phys. Rev. **78**, 182 (1950).
- [41] Y. Takahashi, Nuovo Cim. **6**, 371 (1957).
- [42] A. Ahmad and A. Raya, J. Phys. **G43**, 065002 (2016), arXiv:1602.06448 [hep-ph].



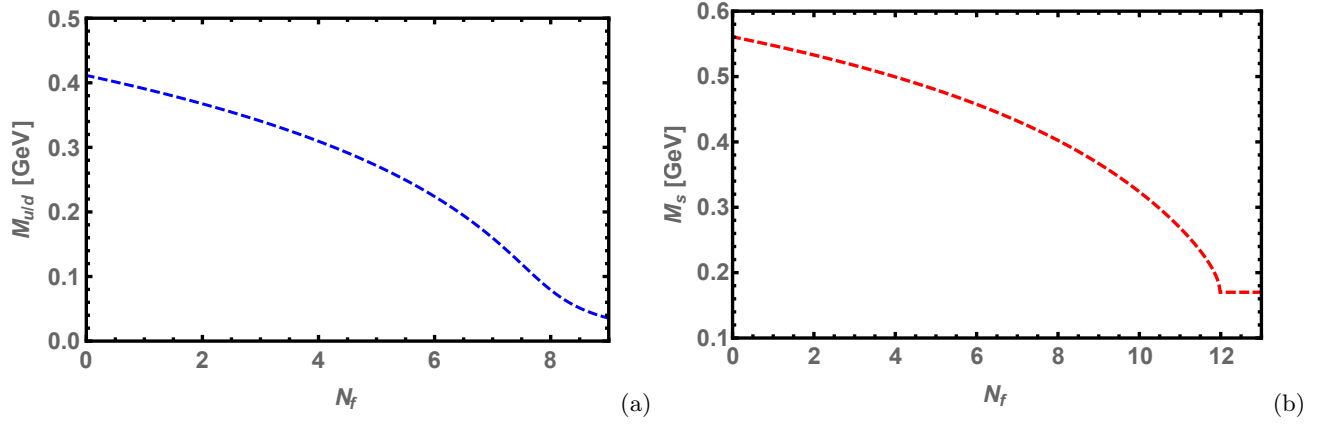


FIG. 5. (a) The dynamical quark mass  $M_{u/d}$  as a function of number of flavors  $N_f$  for fixed  $N_c = 3$  with  $m_{u/d} = 0.007$  GeV. The mass decreases monotonically as we increase  $N_f$  which clearly indicates that the chiral symmetry restored above some critical number of flavors  $N_f^c = 8$ . (b) The behavior of the dynamical strange quark mass  $M_s$  as a function of  $N_f$ , while keeping  $N_c = 3$  fixed with bare strange quark mass  $m_s = 0.17$  GeV. The  $M_s$  decreases as we increase  $N_f$ .

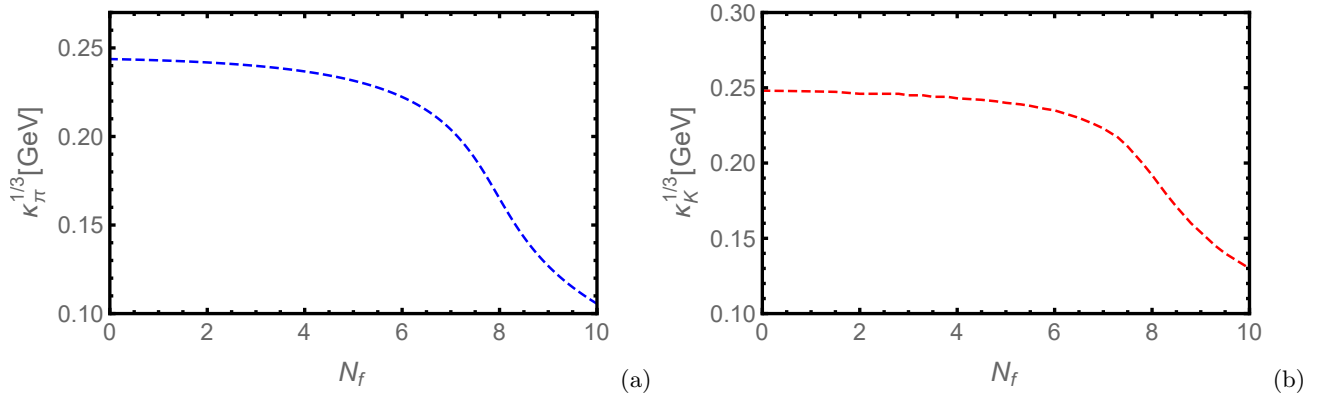


FIG. 6. (a) The pion condensate  $\kappa_\pi^{1/3}$  as a function of number of flavors  $N_f$  for fixed  $N_c = 3$ . It decrease as we increase  $N_f$ . (b) Behavior of the kaon condensate  $\kappa_K^{1/3}$  as a function of  $N_f$ , for fixed  $N_c = 3$ . The  $\kappa_K^{1/3}$  decreases as we increase  $N_f$ .

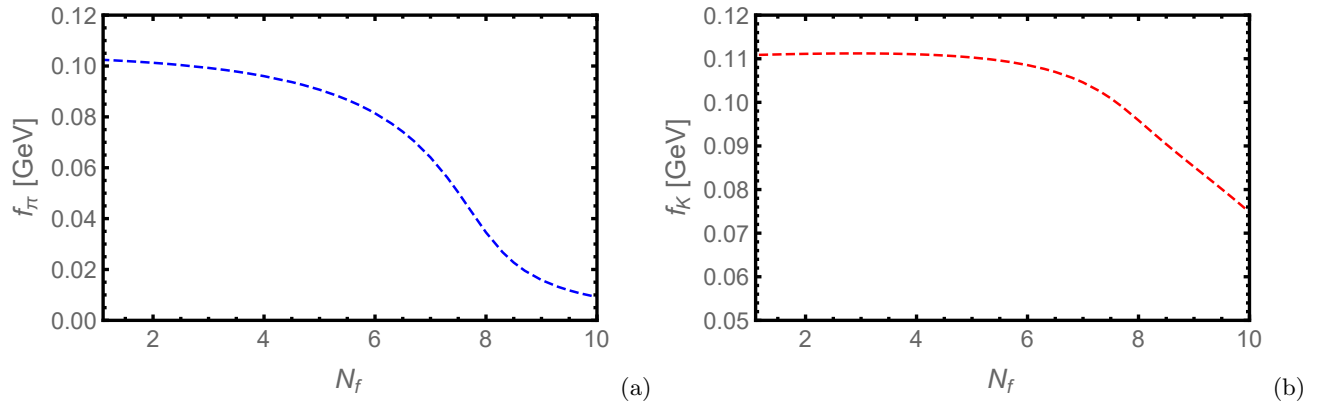


FIG. 7. (a) The evolution of pion decay constant  $f_\pi$  as a function of  $N_f$  for fixed  $N_c = 3$ . The Pion decay constant decreases as we increase  $N_f$ . (b) The evolution of the kaon decay constant  $f_K$  as a function of  $N_f$ , while keeping  $N_c = 3$  fixed. The  $f_K$  decreases as we increase  $N_f$ .

TABLE III. Dynamical generated quark mass of up( $u$ ), down( $d$ ) and strange ( $s$ ) quarks, masses of  $\pi$ -and  $K$ -mesons, the pion decay constant  $f_\pi$ , the kaon decay constant  $f_k$  and their condensates ( $\kappa_\pi^{1/3}$ ) and ( $\kappa_k^{1/3}$ ) for higher number of colors  $N_c$  for fixed  $N_f = 2$ .

$N_c$	$M_{u/d}$	$M_s$	$m_\pi$	$m_k$	$f_\pi$	$f_k$	$\kappa_\pi^{1/3}$	$\kappa_k^{1/3}$
3	0.367	0.533	0.139	0.499	0.101	0.111	0.243	0.247
4	0.520	0.637	0.137	0.515	0.144	0.149	0.278	0.277
5	0.618	0.713	0.139	0.530	0.177	0.180	0.300	0.298
6	0.689	0.722	0.140	0.542	0.204	0.207	0.316	0.313
7	0.745	0.820	0.385	0.552	2.837	0.231	0.329	0.326
8	0.792	0.860	0.576	0.646	0.260	2.052	0.340	0.336
9	0.831	0.895	0.703	0.747	0.287	0.283	0.349	0.346
10	0.866	0.926	0.800	0.829	0.313	0.308	0.358	0.354

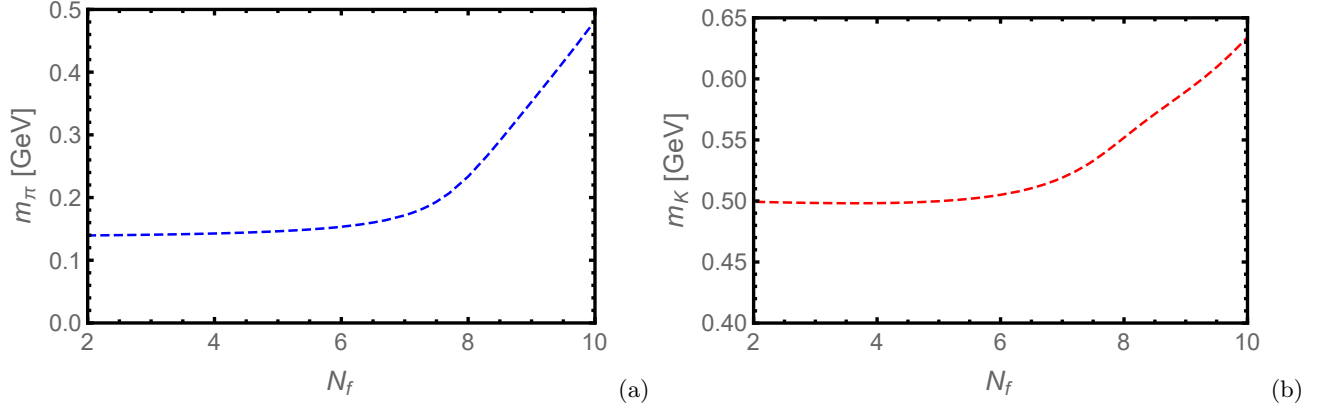


FIG. 8. (a) The mass of pion  $m_\pi$  as a function of number of flavors  $N_f$ , for fixed  $N_c = 3$ . The  $m_\pi$  grows faster near and above  $N_f^c \approx 8$  where the chiral symmetry restoration occurs. (b) The behavior of the Kaon mass  $m_K$  as a function of  $N_f$ , while keeping  $N_c = 3$ . The  $m_K$  Slightly increases as as we increase  $N_f$  and near and above  $N_f^c \approx 8$ , it grows faster.

TABLE IV. Dynamically generated quark mass of up( $u$ ), down( $d$ ) and strange ( $s$ ) quarks, masses of  $\pi$ -and  $K$ -mesons, the pion decay constant  $f_\pi$ , the kaon decay constant  $f_k$  and their in-condensates ( $\kappa_\pi^{1/3}$ ) and ( $\kappa_k^{1/3}$ ) for higher number of flavors  $N_f$  for fixed  $N_c = 3$ .

$N_f$	$M_{u/d}$	$M_s$	$m_\pi$	$m_k$	$f_\pi$	$f_k$	$\kappa_\pi^{1/3}$	$\kappa_k^{1/3}$
2	0.367	0.533	0.139	0.499	0.101	0.111	0.243	0.247
3	0.340	0.517	0.140	0.498	0.099	0.111	0.240	0.245
4	0.309	0.499	0.142	0.498	0.095	0.111	0.236	0.243
5	0.271	0.479	0.146	0.499	0.090	0.110	0.230	0.240
6	0.223	0.457	0.153	0.505	0.081	0.108	0.221	0.235
7	0.158	0.432	0.172	0.519	0.063	0.104	0.202	0.223
8	0.077	0.402	0.235	0.551	0.034	0.095	0.163	0.192
9	0.035	0.366	0.352	0.589	0.015	0.085	0.126	0.154
10	0.020	0.323	0.481	0.634	0.009	0.074	0.105	0.130

- [43] A. Ahmad, Chin. Phys. C **45**, 073109 (2021), arXiv:2009.09482 [hep-ph].
- [44] A. Ahmad, M. Azher, and A. Raya, Eur. Phys. J. A **59**, 252 (2023), arXiv:2308.13210 [hep-ph].
- [45] P. Maris, C. D. Roberts, and P. C. Tandy, Phys. Lett. B **420**, 267 (1998), arXiv:nucl-th/9707003.
- [46] H. L. L. Roberts, C. D. Roberts, A. Bashir, L. X. Gutiérrez-Guerrero, and P. C. Tandy, Phys. Rev. **C82**, 065202 (2010), arXiv:1009.0067 [nucl-th].
- [47] M. A. Bedolla, J. J. Cobos-Martínez, and A. Bashir, Phys. Rev. D **92**, 054031 (2015), arXiv:1601.05639 [hep-ph].
- [48] K. Raya, M. A. Bedolla, J. J. Cobos-Martínez, and A. Bashir, Few Body Syst. **59**, 133 (2018), arXiv:1711.00383 [nucl-th].
- [49] L. X. Gutiérrez-Guerrero, A. Bashir, M. A. Bedolla, and E. Santopinto, Phys. Rev. D **100**, 114032 (2019), arXiv:1911.09213 [nucl-th].
- [50] C. Chen, L. Chang, C. D. Roberts, S. M. Schmidt, S. Wan, and D. J. Wilson, Phys. Rev. C **87**, 045207 (2013), arXiv:1212.2212 [nucl-th].
- [51] S. J. Brodsky, C. D. Roberts, R. Shrock, and P. C. Tandy, Phys. Rev. C **85**, 065202 (2012), arXiv:1202.2376 [nucl-th].
- [52] C. Chen, L. Chang, C. D. Roberts, S. Wan, and D. J. Wilson, Few Body Syst. **53**, 293 (2012), arXiv:1204.2553 [nucl-th].
- [53] Z. Xing and L. Chang, Phys. Rev. D **107**, 014019 (2023), arXiv:2210.12452 [hep-ph].
- [54] R. J. Hernández-Pinto, L. X. Gutiérrez-Guerrero, A. Bashir, M. A. Bedolla, and I. M. Higuera-Angulo, Phys. Rev. D **107**, 054002 (2023), arXiv:2301.11881 [hep-ph].
- [55] G. A. Contrera, D. G. Dumm, and N. N. Scoccola, Phys. Rev. D **81**, 054005 (2010), arXiv:0911.3848 [hep-ph].
- [56] J. L. Flores-Pon, M. A. Bedolla, P. Sloane, and A. Raya, Rev. Mex. Fis. Suppl. **4**, 021124 (2023).